

# Energy and Exergy Analysis of a Geothermal Sourced Multigeneration System for Sustainable City

Sheikh Muhammad Ali Haider <sup>1</sup>, Tahir Abdul Hussain Ratlamwala <sup>1</sup>, Khurram Kamal <sup>1</sup>, Fahad Alqahtani <sup>2,\*</sup>, Mohammed Alkahtani <sup>2</sup>, Emad Mohammad <sup>3</sup> and Moath Alatefi <sup>2</sup>

<sup>1</sup> National University of Sciences and Technology, Islamabad 44000, Pakistan

<sup>2</sup> Industrial Engineering Department, College of Engineering, King Saud University, Riyadh 11421, Saudi Arabia

<sup>3</sup> Electrical Engineering Department, College of Engineering, King Saud University, Riyadh 11421, Saudi Arabia

\* Correspondence: afahad@ksu.edu.sa

**Abstract:** The issue of depleting fossil fuels has emphasized the use of renewable energy. Multigeneration systems fueled by renewables such as geothermal, biomass, solar, etc., have proven to be cutting-edge technologies for the production of different valuable by-products. This study proposes a multigeneration system using a geothermal source of energy. The main outputs include power, space heating, cooling, fresh and hot water, dry air, and hydrogen. The system includes a regenerative Rankine cycle, a double effect absorption cycle and a double flash desalination cycle. A significant amount of electrical power, hydrogen and fresh water is generated, which can be used for commercial or domestic purposes. The power output is 103 MW. The thermal efficiency is 24.42%, while energetic and exergetic efficiencies are 54.22% and 38.96%, respectively. The COP<sub>en</sub> is found to be 1.836, and the COP<sub>ex</sub> is found to be 1.678. The hydrogen and fresh water are produced at a rate of 0.1266 kg/s and 37.6 kg/s, respectively.

**Keywords:** multigeneration system; geothermal; hydrogen; power; renewable



**Citation:** Haider, S.M.A.; Ratlamwala, T.A.H.; Kamal, K.; Alqahtani, F.; Alkahtani, M.; Mohammad, E.; Alatefi, M. Energy and Exergy Analysis of a Geothermal Sourced Multigeneration System for Sustainable City. *Energies* **2023**, *16*, 1616. <https://doi.org/10.3390/en16041616>

Academic Editor: Muhammad Aziz

Received: 22 December 2022

Revised: 20 January 2023

Accepted: 21 January 2023

Published: 6 February 2023



**Copyright:** © 2023 by the authors. Licensee MDPI, Basel, Switzerland. This article is an open access article distributed under the terms and conditions of the Creative Commons Attribution (CC BY) license (<https://creativecommons.org/licenses/by/4.0/>).

## 1. Introduction

Over the past few decades, energy demand has increased exponentially. The increasing population and rising standards of living are its leading causes. Studies show that the world population is growing daily, increasing energy demand [1]. With each day that passes, fossil fuels are nearer to being drained [2]. The world is now concerned with finding alternative ways to produce energy. The Intergovernmental Panel on Climate Change (IPCC) has warned the world that if current practices are not taken into custody, the consequences will be too harsh to handle [3]. Global warming has increased at an unprecedented rate in mankind's history. Two suggestions that have been made in response to this problem include using renewable resources and using efficient methods to generate energy. These practices can lead us to environmentally friendly and cost-effective ways of producing power [4,5].

Global energy generation from fossil fuels leads to extensive CO<sub>2</sub> emissions. Renewables tend to counter this problem. According to the International Energy Agency (IEA), significant carbon dioxide emissions result from burning coal and oil. Other criteria pollutants emitted by fossil fuels, as listed by the Environmental Protection Agency (EPA), USA, include carbon monoxide (CO), oxides of sulfur (SO<sub>x</sub>), oxides of nitrogen (NO<sub>x</sub>), lead (Pb) and particulate matter (PM). Conventional power plants based on fossil fuel also add to the emission of non-criteria pollutants such as hydrocarbons. A considerable increase in energy demand was experienced from 2011 to 2022, in which energy requirements increased by 100% [6,7]. With this rising energy demand, alternative sources must be explored. The studies published in the past two decades show that the world is interested in geothermal sources as a second option for power generation. The demand for energy of the rising

population needs to be fulfilled by alternative energy generation methods, among which geothermal resources stand first.

Renewables are a great source for producing energy. By 2035, renewable energy is expected to be the most important source of energy generation, with an annual rise of about 3%. Renewable energy consumption is expected to treble by 2035 [8]. Considering renewables as a source, multigenerational systems are of great relevance. A multigenerational system (MGS) is a system which produces multiple outputs while having one or multiple primary sources. This system's main goal is to reduce energy waste and increase performance. These systems are better because they not only produce power but also some by-products, such as hydrogen gas, potable water, space heating, etc., in significant amounts which can be used for different purposes. For instance, take a system which produces power by using a high-temperature source and dumping the waste heat into a low-temperature heat sink.

The product of this system would not be limited to power or energy only if the wasted heat is again utilized for space heating or other purposes, increasing the system's efficiency. A study by Towhid et al., in which the Kalina cycle generates power, states that the thermal exergetic efficiencies are 62.79% and 33.82%, respectively, for a source temperature of 160.5 °C. Geothermal and LNG cold energy are their primary sources [9]. Hosein et al. proposed a multigeneration system which also uses Kalina. The main outputs are hydrogen, power and cooling. The system produces 258.6 kW of cooling with a thermal efficiency of 22.28%. The authors stated that if the evaporator's temperature is increased, no significant effect is observed on power production [10].

Fatih et al. have proposed a double flash binary power plant multigeneration system (MGS). Their study shows that high-temperature values enhance the system's performance while a higher flash pressure reduces efficiency, which is an important issue [11]. A flash binary geothermal system was proposed by Kun Li et al. which, along with producing 782 kW of power, is a cost-effective and efficient system [12]. The geothermal source used would have a limited efficiency due to the Carnot Factor. Studies show that a typical geothermal source has efficiencies somewhere between 9.5% and 18%, which means that approximately 85% of the energy is wasted. Not only does MGS produce by-products, but it also reduces energy waste, leading to a considerable boost in the system's efficiency [5]. Farayi, Shoaib and Rasikh have investigated different configurations of a multigeneration system and found out that the part of the system, the absorber in their case, which accepts heat at first has the highest exergy destruction and that its exergy efficiency is low [13]. Moreover, Ali et al. stated that deeper wells have a higher tendency to increase system efficiency compared to other wells that are not as deep [14]. Sameer et al. affirmed in their study that when a geothermal source's temperature increases, the fresh water production rate decreases, which is an important parameter to be considered [15].

A study of the combined effect of cooling, heating and power (CCHP) using an air-cooled cascade system conducted by Nattaporn et al. shows that the system has higher efficiency regarding the first law of thermodynamics and a lower efficiency regarding the second law, which indicates the thermodynamic aspects of the system [16]. Yan et al. developed a system that produced 1.264 GWh of energy with an energy efficiency of 60% and exergetic efficiency of 21%. They found out that when there is an increase in geo-fluid mass flow rate, the power output increases and exergetic efficiency decreases. On the contrary, when there is an increase in  $m$  of sea water, the phenomenon is reversed from the previous one as the power output and exergetic efficiencies decrease [17]. Hojat et al. multi-optimized a multigenerational system to produce energy, water and hydrogen gas using renewables along with liquefied natural gas (LNG) as primary sources along with an evolutionary algorithm. This system's exergetic efficiency is 52.65% with a cost of USD 4.35/GJ [18].

The effect of geothermal source temperature has an eminent impact on output values. Power production and efficiency also depend on the cycles used. A study conducted by Murat and Dincer on a geothermal sourced plant with an added option of storage for six

outputs stated that if the temperature of reference fluid and geothermal fluid temperature is increased, hydrogen production can be enhanced. Moreover, they noted that the exergetic efficiency increases if fluid mass per unit of time increases [19]. Shahid et al. studied MGS, having combined primary sources of solar and geothermal energy. He has found that a double organic Rankine cycle (2-ORC) system is far better than a single ORC system. The efficiencies of the system using two ORC are 62% and 54%, while for a single ORC system, these are 51% and 22%, respectively, which clearly shows that the 2-ORC system is superior to the 1-ORC system [20]. Olusola et al. stated that the Kalina cycle increases the system's electricity production by 14%. It also increased the system's efficiency from 68.73% to 70.08% [21]. Ratlamwala et al. found that three factors are responsible for a change in the system's outputs. These are ambient temperature, solar irradiance, and temperature gradient [22]. Different studies conducted by various researchers tell us about other aspects of the system. Mohammad et al. found out that if the turbine's expansion ratio was high, the exergy efficiency would be higher. Linda et al. found the system's thermal efficiency to be 37.85%, having sources from Salaban geothermal wells with a temperature range of 170–210 °C. Monu et al. researched a multigeneration system and found that the most considerable exergy destruction was in the boiler and combustion chamber. He found the system's exergetic efficiency to be equal to 20% while using the organic Rankine cycle [23–25].

Bozgeyik et al. did a performance analysis of two systems; one of them was a single-generation system, and the other one was a multigeneration system. The single output generating system had energetic and exergetic efficiencies of 13.7% and 50%, respectively, which were lower than the MGS's efficiencies of 98.6% and 67.7%. This contrast highlights the significance of MGS [26]. Fahad et al. analyzed a solar plus geothermal sourced MGS having 54.7% and 76.4% as energy and exergy efficiencies, respectively. The COP of energy and exergy were 0.77 and 0.41, respectively. He further found that source temperature is the most influential element in a system [27]. Hadi et al. proposed a multigeneration system that produces by-products such as fresh water and electrical power with a thermal efficiency of 94.84% and an exergy efficiency of 47.89%. It was observed that a high evaporation temperature would result in high exergy efficiency [28]. The source temperature is the most influential entity of the system in its efficiency and performance. The temperature range also affects the exergy efficiency. Ratlamwala et al. predicted the rise in exergetic efficiency from 0.20 to 0.28 with an increase in temperature of 100 K. Montaser et al. conducted a review study of different multigeneration systems for hydrogen production and stated that multigeneration systems have a great potential for sound output as compared to conventional methods. The hydrogen generation varied from 6 to 13,500 [kg/h] depending on the type of system used [29–32].

The present study presents a novel multigeneration system which consists of three subsystems: (a) Regenerative Rankine Cycle, which produces power, hydrogen and space heating. The generated electricity can be used for domestic or commercial purposes. Hydrogen can serve as fuel. (b) A double effect vapour absorption cycle, which produces cooling and dry air, which are helpful for domestic purposes. (c) A double flash desalination cycle to distil sea water to fresh potable and hot water, which are very useful for living beings. A comprehensive and novel approach was carried out in this research. This study used an efficient system to conduct a detailed analysis in which mathematical modelling, parametric optimization, and exergy analysis were performed. The working conditions of all the subsystems were considered as well. A mathematical model-solving software, Engineering Equation Solver (EES), was used to carry out thermal and exergetic analysis. Exergy destruction analysis was also carried out.

## 2. System Description

A multigenerational system is a system which produces multiple outputs while having one or two inputs as shown in Figure 1. The system developed in this study is a multigenerational system which creates electrical power, space heating, cooling, dry air, fresh water,

hot water and hydrogen, which may be used for different purposes. The system consists of three subsystems: power cycle, cooling cycle and desalination cycle. The power cycle is the Regenerative Rankine Cycle, the cooling cycle is a double effect vapour absorption cycle and the desalination cycle is a double flash desalination cycle. The source used is dry steam with a temperature of 388 °C (661.15 K) and is located in Cerro Prieto, Mexico [33].

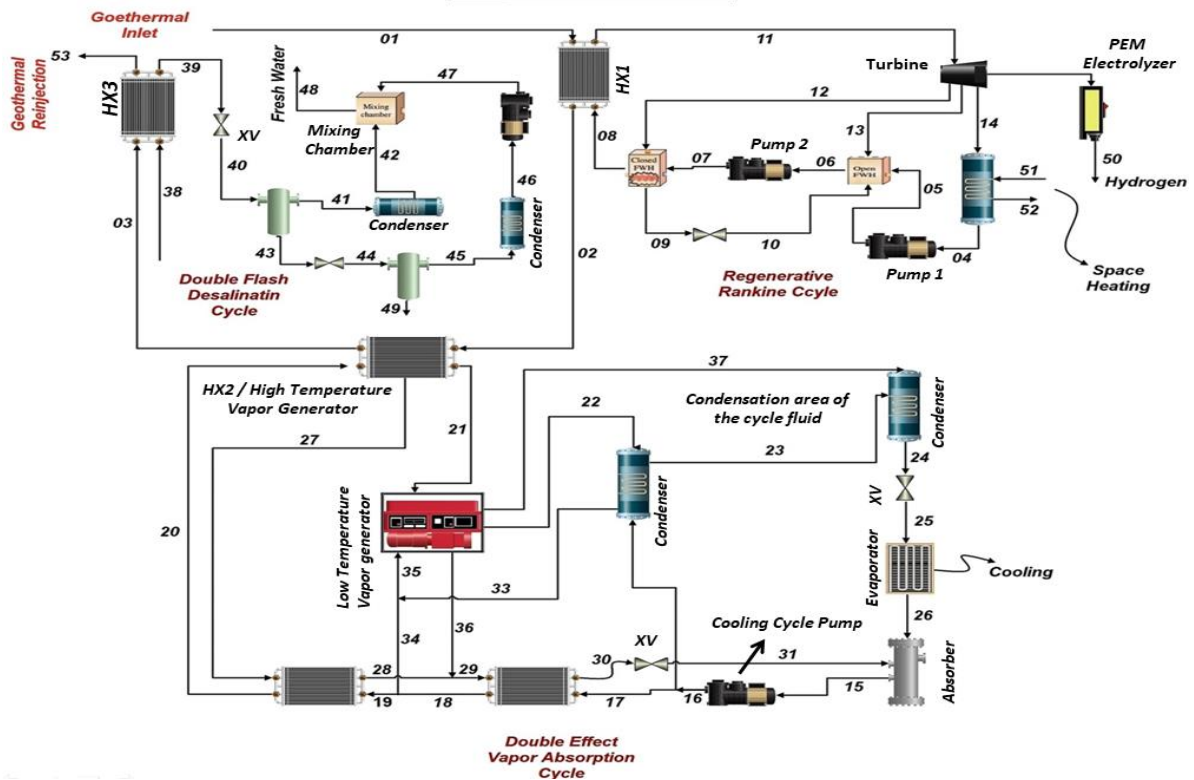


Figure 1. Schematic Diagram of Geothermal Sourced Multigeneration System.

As the name suggests, the power cycle produces electric power, a fraction of which is further used to generate hydrogen. This cycle consists of a heat exchanger, turbine, condenser, two pumps, an expansion valve, a close-feed water heater and an open-feed water heater. An electrolyzer is also attached to the turbine. The geothermal source, dry steam in this case, is extracted from the well at 388 °C with a flow rate of 300 kg/s and is fed to the heat exchanger at 1, as shown in Figure 1, which heats the cycle fluid of the power cycle. The locations where geothermal temperature can exceed 250 °C are Yangbajain, China (250–330 °C), Bedugul, Indonesia (280–330 °C) and Larderello, Italy (300–340 °C). The high-temperature geothermal source was selected to increase the efficiency of the system. An appropriate flow rate value was given, as it is a significant factor for power generation. The studies with similar flow rate values are Karapekmez et al. and Rizvi et al. [33–36]. The heated cycle fluid enters the turbine at state 11 at a higher temperature, producing electricity. A percentage of the electrical power is used to run an electrolyzer which produces hydrogen. The cycle fluid at state 14 is then sent to the condenser to condense it to the liquid state and lower its temperature. The condensed fluid is then fed into a pump at state 4 and sent to the close-feed water heater. A fraction of the cycle fluid is directly sent to the closed FWH, which is pumped (through pump 2) to increase its pressure. The mixing chamber is attached to pump 2 and the closed FWH, where the fluid gets mixed and fed to the first heat exchanger to repeat the procedure. This cycle is repeated to generate electricity and hydrogen.

Heat exchanger 2 controls the cooling cycle, a double effect vapour absorption cycle. A pump, low-temperature HX, high-temperature HX, high-temperature generator (HTG), low-temperature generator (LTG), condenser, condenser (con), expansion valves, evaporator

(eva) and an absorber are all part of the cooling cycle (abs). The pump is where the cycle begins. The absorber's strong solution is pumped to achieve high pressure. The condenser receives 20% of the solution, while the low-temperature heat exchanger receives the remaining 80%, which exchanges heat with the weak solution from the low-temperature vapour generator. The output of the low-temperature heat exchanger (LTHX) is then sent to the high-temperature heat generator (HTHX), from which a fraction of about 20% is removed and sent to the low-temperature vapour generator. The remaining 80% is sent to the high-temperature heat exchanger, which exchanges heat with the heated weak solution from the high-temperature vapour generator (HTG), before being sent to the high-temperature generator to exchange heat with heat exchangers. This ammonia–water ( $\text{NH}_3\text{-H}_2\text{O}$ ) solution is separated into two halves after receiving heat from a geothermal source. The first goes into the low-temperature generator (LTG), while the second goes into the high-temperature heat exchanger. The initial half of the solution is supplied to the condenser, then sent to the condenser again to reject heat to the environment. The weak component of the ammonia–water solution is then passed via a high-temperature heat exchanger before being transferred to a low-temperature heat exchanger. The pressure of the weak solution is dropped by the expansion valve attached to the low-temperature heat exchanger's output for it to mix with the strong solution from the evaporator. The strong solution sent to the condenser is redirected to a condenser, where it is condensed and transmitted to an expansion valve whose sole function is to expand the solution. This enlarged solution is then put into an evaporator, which absorbs heat from the surroundings before being fed into an absorber. The strong and weak solutions are combined and the cycle begins again. The cooling is produced by the cooling cycle's evaporator, which has a capacity of 1125 kJ/s.

The double flash desalination cycle consists of a heat exchanger, two separators, two expansion valves, two condensers, a pump, and a mixing chamber. The geothermal source and salt water are fed to the heat exchanger 3. A geothermal source from heat exchanger 2 is used to heat up the saltwater passing through heat exchanger 3. The geothermal source is then re-injected into the ground. After being heated, the saltwater is fed to an expansion valve, which expands and is inserted into the separator where the liquid and vapour are separated. The liquid produced is fresh water. The remaining vapour from separator 1 is then expanded through expansion valve 2, and then the liquid is separated by separator 2, which is condensed through a condenser. The condenser's output liquid has a comparatively lower pressure than the output liquid of separator 1. So, a pump is used to increase pressure at the outlet of the condenser, which is then sent to the mixing chamber. The outputs of separator 1 and the condenser are mixed in the mixing chamber, and fresh water is produced, which may be used for domestic purposes. The electrolyzer operates by using a fraction of the power produced by the Regenerative Rankine Cycle. This subsystem has 56% efficiency [37].

### 3. Analysis

The current study presents an MGS which has been analyzed thermodynamically. The necessary temperatures and pressures have been supposed at each state. The following assumptions have been made to propose this model [15]:

- Pressure drops across all pumps are neglected.
- The ambient state has a temperature  $T_0 = 30\text{ }^\circ\text{C}$  and pressure 101.325 kPa.
- The turbine and pump have 80% and 50% isentropic efficiencies, respectively.
- The geothermal source temperature is 388  $^\circ\text{C}$ .
- The source mass flow rate is 300 kg/s.
- The electrolyzer has an efficiency of 0.56 or 56%.

The assumptions made here are similar to the assumptions proposed by Cengel [5] for the thermodynamic analysis of a system and to the study conducted by Yuksel et al. [36,37]. The efficiencies of each subsystem, i.e., power cycle, fresh water, cooling cycle, hydrogen, etc., are also evaluated. The first and second law COPs of the cooling cycle are also

calculated. A thermodynamics software engineering equation solver is used to perform the calculations.

### 3.1. Equations

The general equation of the energy balance is as follows:

$$\sum \dot{m}_{in} h_{in} + \dot{W}_{in} + \dot{Q}_{in} = \sum \dot{m}_{out} h_{out} + \dot{W}_{out} + \dot{Q}_{out} \quad (1)$$

Exergies at different points are calculated by:

$$ex_i = m_i * (h_i - h_0) - T_0(s_i - s_0) \quad (2)$$

$$\dot{E}x_i = m_i * ex_i \quad (3)$$

where  $ex_i$  = Specific exergy at state  $i$ ,  $m_i$  = Mass flow rate at state  $i$ ,  $h_i$  = Enthalpy at state  $i$ ,  $h_0$  = Enthalpy at ambient state,  $T_0$  = Temperature at ambient state,  $s_i$  = Entropy at state  $i$ ,  $s_0$  = Entropy at ambient state and  $\dot{E}x_i$  = Exergy at state  $i$ .

Whereas the exergy balance equation is:

$$\sum \dot{E}x_{in} + \dot{W}_{in} + \left(1 - \frac{T_0}{T_{in}}\right) * \dot{Q}_{in} = \sum \dot{E}x_{out} + \dot{W}_{out,turb} + \left(1 - \frac{T_0}{T_{out}}\right) * \dot{Q}_{out} + \dot{E}x_{des} \quad (4)$$

#### 3.1.1. Regenerative Rankine Cycle

In the power cycle, the turbine produces electricity. The turbine efficiency is calculated with the help of Equation (5):

$$\eta_{th} = 1 - \frac{\dot{Q}_{con}}{\dot{Q}_{boi}} \quad (5)$$

where  $\dot{Q}_{con}$  and  $\dot{Q}_{boi}$ , are the heat transfers in the condenser and boiler, respectively. The relations to find these values are as follows.

$$\dot{Q}_{con} = \dot{m}_{14}(h_{14} - h_4) \quad (6)$$

$$\dot{Q}_{boi} = \dot{m}_{11}(h_{11} - h_8) \quad (7)$$

The turbine work is calculated from the following relation:

$$\dot{W}_{tu} = \dot{m}_{11} * (h_{11} - y * h_{12} - z * h_{13}(1 - y - z) * h_{14}) \quad (8)$$

where  $y$  and  $z$  are the bleeds taken from the turbine's output; their values are calculated from the following equations.

$$y = \frac{h_8 - h_7}{h_{12} - h_{14}} \quad (9)$$

$$z = \frac{(h_6 - h_5) - y(h_{10} - h_{15})}{h_{13} - h_5} \quad (10)$$

$$\dot{W}_{pu} = \dot{m}_4 - (h_5 - h_4) + \dot{m}_6(h_7 - h_6) \quad (11)$$

where  $\dot{m}$  is the mass flow rate and  $h$  is enthalpy at respective states.

The net work performed in the power cycle is calculated by:

$$\dot{W}_{net} = \dot{W}_{tu} - \dot{W}_{pu} \quad (12)$$

where  $\dot{W}_{tu}$  is the net turbine work and  $\dot{W}_{pu}$  is the net pump work of the system.

The exergetic efficiency of the power cycle is calculated by:

$$\eta_{ex,power} = \frac{\dot{W}_{net}}{\left(1 - \frac{T_0}{T_{11}}\right) * \dot{Q}_{boi}} \quad (13)$$

### 3.1.2. Double Effect Vapour Absorption Cycle

The exergetic coefficient of performance is calculated by the following equation:

$$COP_{ex} = \frac{\dot{E}x_{th,eva}}{\dot{E}x_{HTG} + \dot{W}_{pu}} \quad (14)$$

where  $\dot{E}x_{th,eva}$  is the thermal exergy of the evaporator,  $\dot{E}x_{HTG}$  is the exergy of a high-temperature vapour generator and  $\dot{W}_{pu}$  is the work done by the pump, calculated by the following expression:

$$\dot{W}_{pu} = \dot{m}_{15}(h_{16} - h_{15}) \quad (15)$$

The following relation calculates the COP of energy.

$$COP_{en} = \frac{\dot{Q}_{eva}}{\dot{Q}_{HTG} - \dot{W}_p} \quad (16)$$

$$\dot{W}_p = \dot{m}_{15} * (h_{16} - h_{15}) \quad (17)$$

where  $\dot{Q}_{eva}$  is the heat transfer rate of the evaporator and  $\dot{Q}_{HTG}$  is the heat transfer rate of the high-temperature generator.

The relations for the evaporator and high-temperature heat exchanger exergies are given as:

$$\dot{E}x_{th,eva} = \left(1 - \frac{T_0}{T_{eva}}\right) * \dot{Q}_{eva} \quad (18)$$

$$\dot{E}x_{th,HTG} = \left(1 - \frac{T_0}{T_{HTG}}\right) * \dot{Q}_{HTG} \quad (19)$$

### 3.1.3. PEM Electrolyzer

The following expression calculates hydrogen production efficiency.

$$\eta_{hyd} = \frac{\dot{m}_{hyd} * HHV_{hyd}}{\dot{W}_{electrolyzer}} \quad (20)$$

where  $\dot{m}_{hyd}$  is the mass flow rate of hydrogen produced,  $HHV_{hyd}$  is the high heating value of hydrogen and  $\dot{W}_{electrolyzer}$  is the net work output of the PEM electrolyzer.

The following expression calculates the exergy of hydrogen:

$$ex_{hyd} = ex_{ch} + ex_{phy} \quad (21)$$

where  $ex_{ch}$  is the chemical exergy of hydrogen and  $ex_{phy}$  is the physical exergy of hydrogen. The relation for chemical exergy is:

$$ex_{ch} = (236100) / \text{molarmass}_{hydrogen} \quad (22)$$

$$ex_{phy} = \left[ (h_{hydrogen} - h_0) - T_0 (s_{hydrogen} - s_0) \right] \quad (23)$$

The expressions for hydrogen's chemical and physical exergy are taken from [22].

### 3.1.4. Space Heating

$$\dot{Q}_{cond,heating} = \dot{m}_{51} * cp_{air} * (T_{52} - T_{51}) \quad (24)$$

### 3.1.5. Double Flash Desalination Cycle

$$\eta_{en, fw} = \frac{\dot{m}_{43}h_{43} + \dot{m}_{46}h_{46} + \dot{m}_{49}h_{49} - \dot{m}_{38}h_{38}}{\dot{Q}_{SW}} \quad (25)$$

$$\eta_{ex} = \frac{\dot{E}x_{48} + \dot{E}x_{49} - \dot{E}x_{38}}{\left(1 - \frac{T_0}{T_3}\right) * \dot{Q}_{SW}} \quad (26)$$

The fresh water produced is calculated by:

$$\dot{m}_{fw} = \frac{\dot{m}_{45}h_{45} + \dot{m}_{47}h_{47}}{h_{48}} \quad (27)$$

The fresh water is being produced at a considerable temperature, i.e., 40 °C, which can be used as hot water as it is being generated. Hence, a fraction of fresh water would be extracted for hot water.

$$\dot{m}_{hw} = \frac{\dot{m}_{48}}{2} \quad (28)$$

### 3.1.6. Overall Energy and Exergy Efficiency

The energetic efficiency of the system is calculated by:

$$\eta_{en, sys} = \frac{\dot{W}_{net} + \dot{m}_{48}h_{48} + \dot{Q}_{eva} + \dot{m}_{52}(h_{52} - h_{51})}{\dot{m}_1h_1 + \dot{W}_{pu}} \quad (29)$$

where  $\eta_{en, sys}$  is the energy efficiency of the system,  $\dot{W}_{net}$  is the net power output from the power cycle,  $\dot{m}_{48}h_{48}$  is the rate of energy transfer by fresh water from the double stage flash desalination cycle,  $\dot{Q}_{eva}$  is the rate of cooling from the double effect vapour absorption cycle,  $\dot{m}_{52}(h_{52} - h_{51})$  is the rate of energy transfer to cold air for space heating,  $\dot{m}_1h_1$  is the rate of energy input to the multigeneration system by the geothermal source and  $\dot{W}_{pu}$  is the net pump work of the entire system.

The exergetic efficiency is calculated by the following relation:

$$\eta_{ex, sys} = \frac{\dot{W}_{net} + \left(1 - \frac{T_0}{T_{14}}\right) * \dot{Q}_{con} + \left(1 - \frac{T_0}{T_{25}}\right) \dot{Q}_{eva} + \dot{m}_{48}ex_{48}}{\dot{m}_1h_1 + \dot{W}_{pu}} \quad (30)$$

where  $\eta_{ex, sys}$  is the exergetic efficiency of the system,  $\left(1 - \frac{T_0}{T_{14}}\right) * \dot{Q}_{con}$  is the thermal exergy of space heating,  $\left(1 - \frac{T_0}{T_{25}}\right) \dot{Q}_{eva}$  is the thermal exergy of space cooling and  $\dot{m}_{48}ex_{48}$  is the exergy of fresh water.

### 3.1.7. Exergy Destruction (System)

The exergy destruction  $\dot{E}x_{des,sys}$  is calculated by the following equation.

$$\begin{aligned} \dot{m}_1ex_1 + \dot{W}_{pu} + \dot{m}_{48}ex_{48} + \left(1 - \frac{T_0}{T_{26}}\right) \dot{Q}_{eva} \\ = \dot{m}_{53}h_{53} + \dot{W}_{tu} + \dot{m}_{47}ex_{47} + \left(1 - \frac{T_0}{T_{24}}\right) * \dot{Q}_{cond} + \left(1 - \frac{T_0}{T_{14}}\right) * \dot{Q}_{con} + \dot{E}x_{des,sys} \end{aligned} \quad (31)$$

where  $\dot{m}_1 ex_1$  is the geothermal source exergy input to the system,  $\dot{m}_{53} h_{53}$  is the exergy out of the system and back to the geothermal source,  $\dot{W}_{tu}$  is the net power output of the turbine,  $\dot{m}_{47} ex_{47}$  is the exergy of brine output from the double stage flash desalination cycle,  $\left(1 - \frac{T_0}{T_{24}}\right) * \dot{Q}_{cond}$  is the heat rejected by the condenser in the cooling cycle and  $\dot{E}x_{des.sys}$  is the exergy destroyed by the system.

#### 4. Results and Discussion

The proposed model produces multiple outputs with a single input, i.e., a geothermal source (dry steam). The outputs include power, heating, cooling, fresh water, hydrogen, dry air and hot water. The main output is power, which can also be used for commercial and domestic purposes. A literature review has been performed to assume input values of temperature and pressure at specific points. The values of mass flow rates were also selected by the method mentioned above. The particular enthalpies and exergies are calculated using enthalpy and exergy functions in Engineering Equation Solver (EES). The multi-level optimization was performed to obtain the most efficient operating conditions. The proposed model is validated by comparing its results to different input conditions used in previous research. The validation of the model confirms its efficacy compared to other systems. This system is designed to use only a geothermal source as its primary and only source, unlike other published studies that use more than one source to produce the same or fewer outputs [38–41]. The current study gives us 103 MW of power, 37.6 kg/s of fresh water and 0.122 kg/s of hydrogen, which are better than the mentioned studies [10,42–44].

EES calculates different parameters like temperature, pressure, enthalpy, entropy, exergy, and mass flow rate at other state points of each cycle. These state points are tabulated in the following.

##### 4.1. State Point Values of the Subsystems

The values of different state points of each subsystem are given in this section.

##### 4.1.1. Geothermal Source

Table 1 consists of all three state points, which are 1, 2 and 3. The geothermal source enters at 1 in heat exchanger 1, rejects some heat to the working fluid of the power cycle and exits. It then enters heat exchanger 2 to heat the cooling process working fluid and heat exchanger 3, from which it is re-injected into the ground from which it was taken.

**Table 1.** State point values of Temperature, Pressure, Enthalpy, Entropy, Exergy and Mass flow rate of Geothermal Source.

State Point	Temperature, T [K]	Pressure, P [kPa]	Enthalpy, h [kJ/kg]	Entropy, s [kJ/kg K]	Exergy, ex [kJ/kg]	Mass Flow Rate, m [kg/s]
1	661	15,000	2992	5.802	1171	300
2	382.4	15,000	469	1.398	51.92	300
3	381.9	15,000	467	1.393	51.51	300

##### 4.1.2. Regenerative Rankine Cycle (Power Cycle)

Table 2 consists of different state point values of the parameters enlisted below. The states included are only for the power production in the power cycle. Hydrogen and space heating are also harnessed through the power cycle but are not included in this table. Mass flow rates of the working fluid of the power cycle at each point are also listed. All the values are obtained from EES.

**Table 2.** State point values of Temperature, Pressure, Enthalpy, Entropy, Exergy and Mass flow rate of Regenerative Rankine Cycle.

State Point	Temperature, T [K]	Pressure, P [kPa]	Enthalpy, h [kJ/kg]	Entropy, s [kJ/kg K]	Exergy, ex [kJ/kg]	Mass Flow Rate, m [kg/s]
4	333.2	20	251.4	0.832	5.826	165.5
5	333.2	100	251.5	0.8321	5.909	165.5
6	372.8	100	417.5	1.303	29.27	211.8
7	374.7	15,000	436.9	1.313	45.52	211.8
8	438.1	15,000	705.3	1.975	113.5	211.8
9	438.1	700	697	1.992	100	35.34
10	372.8	100	697	2.053	81.58	35.34
11	623	15,000	2692	5.442	1049	211.8
12	438.1	700	2305	5.662	595.9	35.34
13	372.8	100	2029	5.627	330.9	10.92
14	333.2	20	2173	6.598	180	165.5

#### 4.1.3. Double Effect Vapour Absorption Cycle (Cooling Cycle)

Table 3 shows the temperature, pressure, enthalpy, entropy, exergy, and mass flow rate values of each state point in the cooling cycle.

**Table 3.** State point values of Temperature, Pressure, Enthalpy, Entropy, Exergy and Mass flow rate of Double Effect Vapour Absorption Cycle.

State Point	Temperature, T [K]	Pressure, P [kPa]	Enthalpy, h [kJ/kg]	Entropy, s [kJ/kg K]	Exergy, ex [kJ/kg]	Mass Flow Rate, m [kg/s]
15	273.9	200	-225.9	-0.1641	72.78	2.5
16	274.1	700	-224.7	-0.1619	73.34	2.5
17	274.1	700	-224.7	-0.1619	73.34	2
18	284.1	700	-178.8	0.002663	69.4	2
19	284.1	700	-178.8	0.002663	69.4	1.6
20	294.1	700	-133.1	0.1606	67.2	1.6
21	287	700	760.5	2.666	303.6	0.6957
22	232.3	700	-183.3	-0.716	0.8637	0.6957
23	229.1	700	-197.6	-0.7783	386.1	0.6957
24	278.9	700	26.49	0.1063	342.2	1.087
25	254.3	200	26.49	0.1274	335.8	1.087
26	265.3	200	1271	4.906	104.9	1.087
27	314.1	700	-9.393	0.5257	1.524	0.9043
28	295.3	700	-90.18	0.2606	1.095	0.9043
29	297.4	700	-81.44	0.29	0.8992	1.413
30	282.4	700	-146.4	0.06571	3.864	1.413
31	282.5	200	-146.4	0.06768	3.269	1.413
32	274.1	700	-224.7	-0.1619	73.34	0.5
33	278.5	700	-204.7	-0.08949	71.4	0.5
34	284.1	700	-178.8	0.002663	69.4	0.4
35	281	700	-193.2	-0.0483	70.45	0.9
36	301	700	-65.91	0.3419	0.6997	0.5086
37	301	700	1319	4.591	276.2	0.3914

#### 4.1.4. Double Flash Desalination Cycle

Table 4 shows each state point's temperature, pressure, enthalpy, entropy, exergy, and mass flow rate values in the desalination cycle.

**Table 4.** State point values of Temperature, Pressure, Enthalpy, Entropy, Exergy and Mass flow rate of Double Flash Desalination Cycle.

State Point	Temperature, T [K]	Pressure, P [kPa]	Enthalpy, h [kJ/kg]	Entropy, s [kJ/kg K]	Exergy, ex [kJ/kg]	Mass Flow Rate, m [kg/s]
38	303	101.3	120.6	0.4204	2.682	287.5
39	388	101.3	464.3	1.42	44.7	287.5
40	319	10	464.3	1.504	15.24	287.5
41	319	10	183.9	0.623	4.337	254.7
42	306	5	183.9	0.457	2.738	254.7
43	306	5	2560	8.393	23.91	4.851
44	306	5	137.8	0.4762	−0.03407	4.851
45	306	10	137.8	0.4762	−0.03407	4.851
46	319	10	2584	8.148	121.23	32.75
47	319	10	191.8	0.6492	1.605	32.75
48	317.3	10	184.8	0.6237	1.274	37.6
49	306	5	131.9	0.4566	2.738	249.9

#### 4.1.5. Hydrogen and Space Heating Production

Table 5 shows the state point values of state 50, where hydrogen is produced. State points 51 and 52 are related to heating production, here termed space heating. Different parametric values were calculated using EES and are tabulated here.

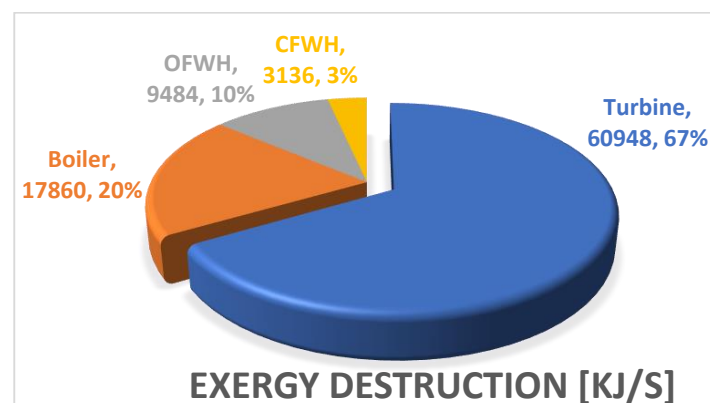
**Table 5.** State point values of Temperature, Pressure, Enthalpy, Entropy, Exergy and Mass flow rate of Hydrogen and Space Heating.

State Point	Temperature, T [K]	Pressure, P [kPa]	Enthalpy, h [kJ/kg]	Entropy, s [kJ/kg K]	Exergy, ex [kJ/kg]	Mass Flow Rate, m [kg/s]
50	303	101.325	69.59	65	117,117	0.1266
51	283	101.325	283.4	5.643	0.6994	15,837
52	303	101.325	303.4	5.712	0	15,837

## 4.2. Exergy Destruction and Energy Efficiencies Calculation

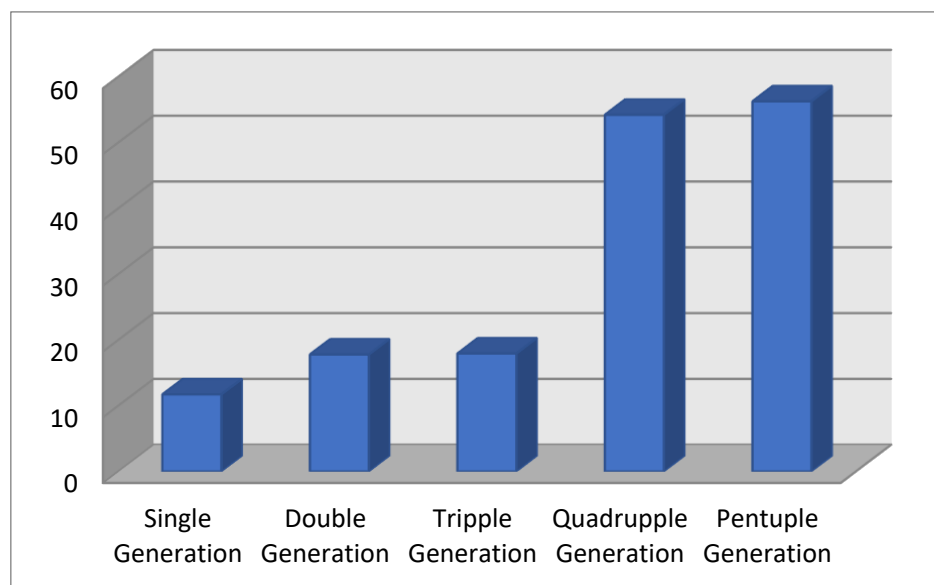
### 4.2.1. Major Exergy Destruction Areas

Figure 2 is a pie chart which shows major exergy destruction areas of the multigeneration system. The comparison includes turbine, boiler, OFWH and CFWH, which were chosen based on higher exergy destruction values. The turbine has maximum exergy destruction, which shows high entropy generation. The closed feedwater heater (CFWH) has the lowest among these four components.

**Figure 2.** Major Exergy Destruction Areas of the Multigeneration System.

#### 4.2.2. Energy Efficiencies at Different Production Loads

Figure 3 shows different energy efficiencies calculated at different production loads of multigeneration system. This comparison is divided into five stages: single generation, meaning only power, double generation, triple generation, quadruple generation and pentuple generation. It can be visualized that the system is more efficient when more outputs are taken from it, which depicts the significance of multigeneration systems. The system is efficient when more products are harnessed because losses are minimized during the single or double generation process. The geothermal source heat is used more effectively, and more energy is harnessed from it, thus making the system more efficient.



**Figure 3.** Comparative Bar Plot of Different Energy Efficiencies of Multigeneration System at Different Production Capacities.

#### 4.3. Graphical Representation of Results

The system is optimized to attain the best operating conditions to obtain the maximum possible output. EES is used to perform simulation and plot the graphs to check the effect of geothermal source and ambient temperature on different output values. The following figures show different trends of the impact of source temperature on power output, fresh water and hydrogen production, turbine output, etc. The graph trend for the effect of salinity on fresh water and sea water production has also been plotted.

Figure 4 shows the relation of power output with geothermal source temperature. The graph depicts that when the temperature increases, the power output increases as well. There is an exponential increase in the power output when we increase the temperature. For an increase of 100 K from 573 K, the power output increases from 55 MW TO 110 MW, which is a significant increase. The power output is more remarkable because of the higher flow rates through the Regenerative Rankine Cycle. The efficiency of the turbine increases when the source temperature is increased. The reason is the raised area under the curve in the t-s diagram as the fluid gets superheated at higher temperatures.

Figure 5 shows the geothermal source temperature's effect on the turbine's work output in the Regenerative Rankine Cycle (power cycle). When the source temperature increases, more heat is exchanged in the heat exchanger or superheaters. Thus, the working fluid carries more heat than before, resulting in higher turbine inlet temperature and enthalpy. The higher the enthalpy, the higher the work output from the turbine. This is why the graph shows an increasing trend when the source temperature increases.

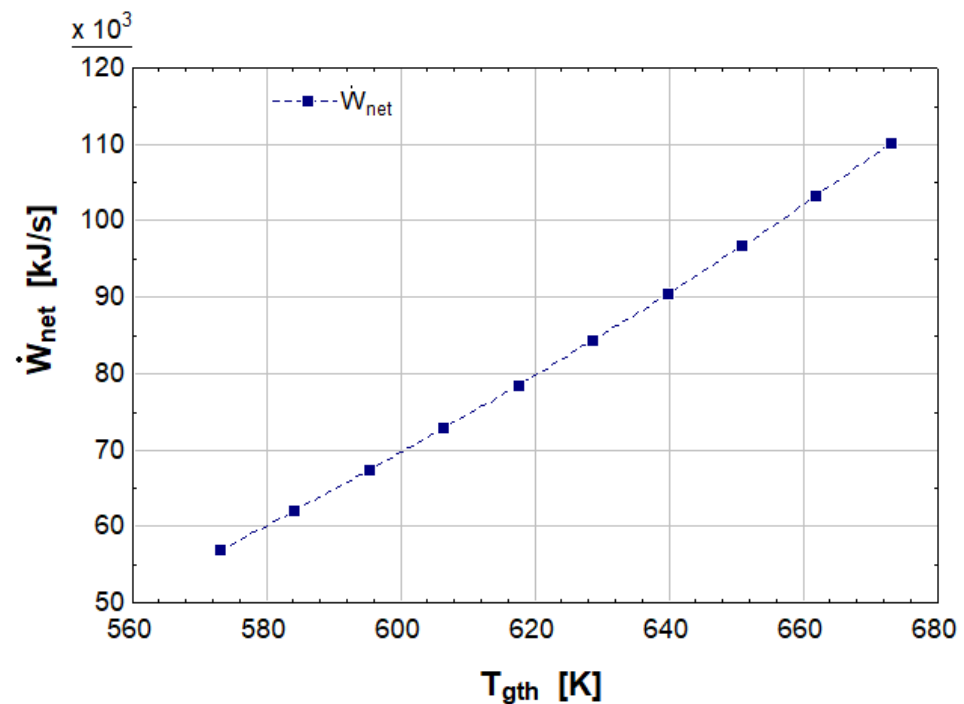


Figure 4. Effect of Geothermal Source Temperature on Net Power Output of System.

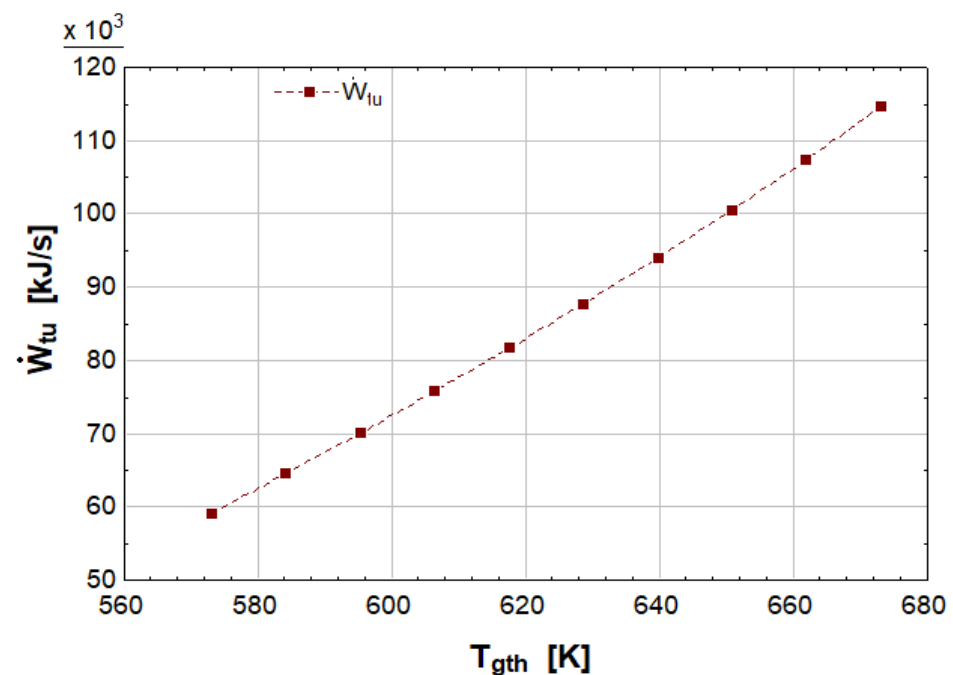


Figure 5. Effect of Geothermal Source Temperature on Turbine Work Output.

In Figure 6, the effect of ambient temperature on the exergy efficiency of the system has been analyzed by plotting the graph. The trend goes downwards, showing that exergy efficiency decreases when the atmospheric or ambient temperature rises. If the exergy efficiency is lowered, the system is not sustainable and hence is considered less efficient. If exergy efficiency is greater, the system is more sustainable and efficient. The ambient temperature significantly affects system output as it directly affects the working of turbines. The increased ambient temperature, especially in hot and dry areas, leads to a lower turbine output, resulting in decreased exergy efficiency.

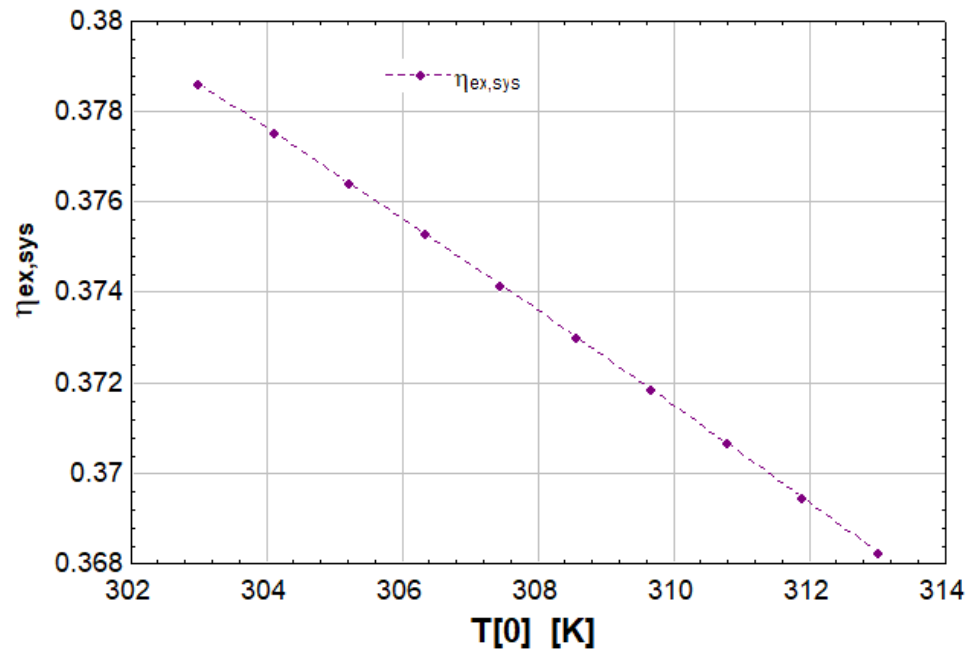


Figure 6. Effect of Ambient Temperature on Exergy Efficiency of Multigeneration System.

The effect of geothermal source temperature on fresh water and hydrogen production is analyzed by plotting the graph shown in Figure 7. An increase in source temperature increases power generation, resulting in enhanced hydrogen production as the PEM electrolyzer takes power directly from the turbine. The higher the temperature, the higher would be the power generation and hydrogen production. On the other hand, fresh water generation reduces when the source temperature increases because of the increased evaporation of water due to high temperature.

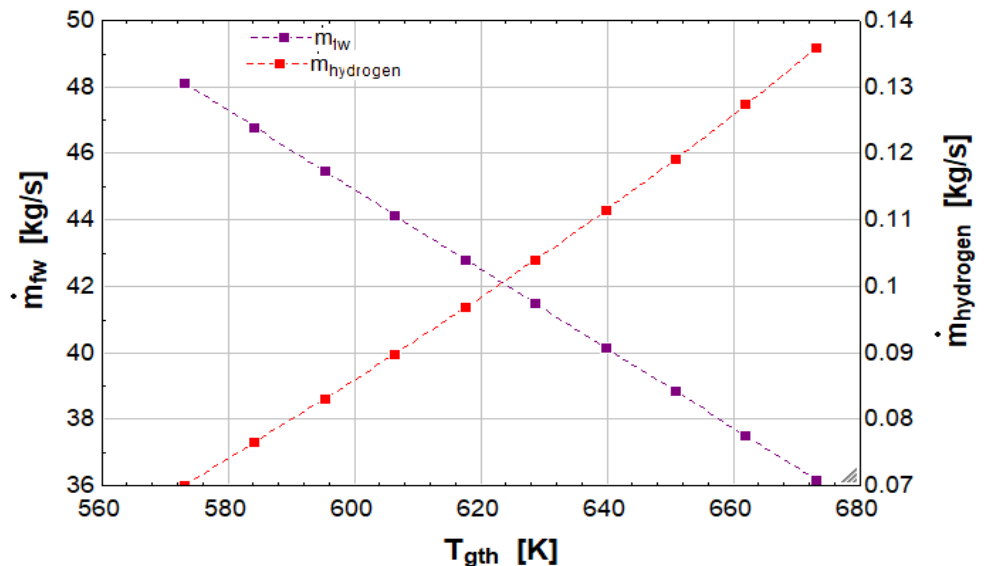


Figure 7. Effect of Geothermal Source Temperature on Fresh Water and Hydrogen Production.

Figure 8 shows the effect of salinity on the production rate of fresh water and sea water (brine) discharge. Salinity tells us the amount of salt in the water. The trends depict that the higher the salinity, the higher is the fresh water produced. On the other hand, salinity reduces the production or discharge of remaining sea water or brine because most of the injected sea water is used in fresh water production. The salinity value varied from 20 g/kg

to 80 g/kg, increasing fresh water production by 4–5 kg/s. The sea water production is reduced by 20 kg/s, which is a significant result.

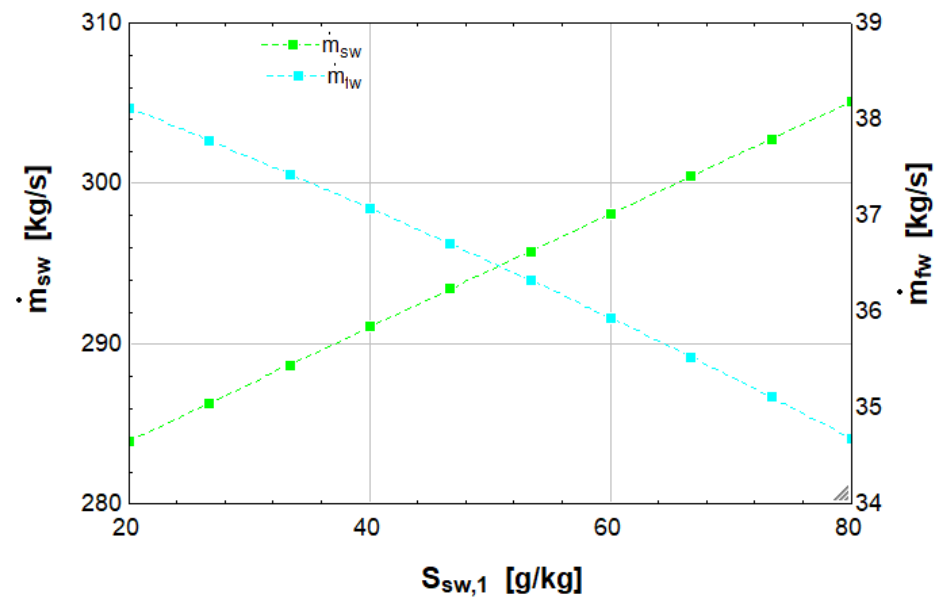


Figure 8. Effect of Salinity on Fresh Water and Sea Water Production.

## 5. Conclusions

In this study, a novel geothermal sourced multigeneration system has been developed, numerically simulated and thermodynamically analyzed to produce power and other by-products such as fresh water, hydrogen, heating, etc. The following conclusions are based on the analysis performed.

- This system produces 103 MW of electricity, the production capacity of which depends on the temperature of the geothermal source. The higher the temperature, the higher would be the power generation.
- The system produces 1.35 MW and 317 MW cooling and heating capacities, respectively. These values depend on the source temperature and the output of the power cycle. Greater output power produces higher heating and cooling.
- Fresh water is produced at a rate of 37.6 kg/s. This fresh water is delivered at 40 °C; hence, a fraction of it can be used as hot water, eliminating the need to produce hot water separately.
- An amount of 0.1266 kg of hydrogen is produced per second through this system which can be transported and used to make fuel cells for automobiles or any other use.
- The system has energy and exergy efficiencies are 54.22% and 38.96%, respectively. At the same time, the coefficients of energy and exergy performance are 1.84 and 1.67, respectively. It is seen that exergy efficiency decreases with an increase in ambient temperature, which is a natural phenomenon—both COPs increase when the source temperature is increased.
- It is seen that the temperature of the geothermal source has the most significance in increasing or reducing the system's performance. This temperature is directly responsible for power production. The higher the source temperature, the higher will be the power output. This affects power output and other products like fresh water and hydrogen production.
- Major exergy destruction areas have also been analyzed. The turbine has the highest exergy destruction rate in the whole system, indicating a significant entropy generation of 60,948 kJ/s.
- Geothermal source temperature affects the production of fresh water and hydrogen. It increases the output of hydrogen generation and vice versa in the case of fresh water.

- Salinity has significant effects on fresh water production. An increasing variation from 20–80 (g/kg) in salinity increases fresh water production by 5 kg/s.

**Author Contributions:** Conceptualization, T.A.H.R. and K.K.; methodology, S.M.A.H.; software, F.A. and M.A. (Mohammed Alkahtani); formal analysis, S.M.A.H., T.A.H.R. and K.K.; investigation, E.M. and M.A. (Moath Alatefi); resources, F.A. and M.A. (Mohammed Alkahtani). All authors have read and agreed to the published version of the manuscript.

**Funding:** The authors extend their appreciation to the Deputyship for Research and Innovation, Ministry of Education in Saudi Arabia, for funding this research work through project no. (IFKSURG-1497).

**Data Availability Statement:** The data presented in this study are available on request from the corresponding author.

**Acknowledgments:** The authors extend their appreciation to the Deputyship for Research and Innovation, Ministry of Education in Saudi Arabia, for funding this research work through project no. (IFKSURG-1497).

**Conflicts of Interest:** The authors declare no conflict of interest.

## Abbreviations

### Symbols

$\eta$	Efficiency
$\dot{m}$	Mass flow Rate
$h$	Enthalpy
$s$	Entropy
$ex$	Specific Exergy
$\dot{E}x$	Exergy Rate
$\dot{W}$	Work Rate
$\dot{Q}$	Heat Rate
$T$	Temperature
$\eta_{th}$	Thermal Efficiency
$\eta_{hyd}$	Hydrogen Production Efficiency
$\eta_{en, fw}$	Energetic Efficiency of Fresh Water
$\eta_{ex}$	Exergy Efficiency
$\dot{m}_{fw}$	Mass Flow Rate of Fresh Water Produced
$\dot{m}_{hw}$	Mass Flow Rate of Hot Water Produced
$\dot{Q}_{con}$	Heat Transfer in Condenser
$\dot{Q}_{boi}$	Heat Transfer in Boiler
$\dot{W}_{tu}$	Turbine Work Output
$y$	Bleed Input to Closed Feed Water Heater
$z$	Bleed Input to Open Feed Water Heater
$\dot{W}_{pu}$	Net Pump Work
$\dot{W}_{net}$	Net Power Output
$\eta_{ex, power}$	Exergy Efficiency of Power Cycle
$COP_{ex}$	Exergetic Coefficient of Performance
$COP_{en}$	Energetic Coefficient of Performance
$\dot{E}x_{th, eva}$	Thermal Exergy of Evaporator
$\dot{E}x_{th, HTG}$	Thermal Exergy of High-Temperature Vapour Generator
$\dot{Q}_{eva}$	Heat Transfer in Evaporator
$\dot{Q}_{HTG}$	Heat Transfer through High-Temperature Generator
$\dot{W}_{electrolyzer}$	Work Output of Electrolyzer
$\dot{Q}_{cond, heating}$	Heat Transfer of Space Heating
$\dot{E}x_{des, sys}$	Exergy Destruction of the System

**Subscripts**

<i>sys</i>	System
<i>abs</i>	Absorber
<i>eva</i>	Evaporator
<i>boi</i>	Boiler
<i>con</i>	Condenser
<i>tu</i>	Turbine
<i>pu</i>	Pump
<i>fw</i>	Fresh Water
<i>hw</i>	Hot Water
<i>sw</i>	Sea Water
<i>en</i>	Energy
<i>ex</i>	Exergy
<i>electro</i>	Electrolyzer
<i>des</i>	Destruction

**Abbreviation**

MGS	Multigeneration System
HX	Heat Exchanger
XV	Expansion Valve
HHX	High-Temperature Heat Exchanger
LHX	Low-Temperature Heat Exchanger
HTG	High-Temperature Generator
COP	Coefficient of Performance
HHV	High Heating Value

**References**

1. United States Census Bureau. U.S. and World Population Clock. United States Census Bureau. 2022. Available online: <https://www.census.gov/popclock/> (accessed on 6 January 2023).
2. Roser, M.; Ortiz-Ospina, E.; Ritchie, H.; Rod s-Guirao, L. "World Population Growth". Our World in Data. 2013. Available online: <https://ourworldindata.org/world-population-growth> (accessed on 6 January 2023).
3. The Intergovernmental Panel on Climate Change: 30 Years Informing Global Climate Action. 13 March 2018. Available online: <https://unfoundation.org/> (accessed on 6 January 2023).
4. IPCC. AR5 Climate Change 2013: The Physical Science Basis—IPCC. 2013. Available online: <https://www.ipcc.ch/report/ar5/wg1/> (accessed on 6 January 2023).
5. Cengel, Y.A.; Boles, M.A. *Thermodynamics: An Engineering Approach 4th Edition in SI Units*; McGraw-Hill: Singapore, 2002.
6. International Energy Agency. IEA—The Global Energy Authority. 2022. Available online: <https://www.iea.org/> (accessed on 6 January 2023).
7. EPA. "US EPA". Available online: <https://www.epa.gov/> (accessed on 6 January 2023).
8. Energy Information Administration. International Energy Outlook 2010. Washington, DC, USA; DOE/EIA-0484(2010). 2021. Available online: <https://www.eia.gov/outlooks/ieo/> (accessed on 6 January 2023).
9. Parikhani, T.; Gholizadeh, T.; Ghaebi, H.; Sadat, S.M.S.; Sarabi, M. Exergoeconomic optimization of a novel multigeneration system driven by geothermal heat source and liquefied natural gas cold energy recovery. *J. Clean. Prod.* **2019**, *209*, 550–571. [[CrossRef](#)]
10. Azariyan, H.; Vajdi, M.; Takeh, H.R. Assessment of a high-performance geothermal-based multigeneration system for production of power, cooling, and hydrogen: Thermodynamic and exergoeconomic evaluation. *Energy Convers. Manag.* **2021**, *236*, 113970. [[CrossRef](#)]
11. Yilmaz, F.; Ozturk, M.; Selbas, R. Modeling and design of the new combined double-flash and binary geothermal power plant for multigeneration purposes; thermodynamic analysis. *Int. J. Hydrogen Energy* **2021**, *47*, 19381–19396. [[CrossRef](#)]
12. Li, K.; Ding, Y.-Z.; Ai, C.; Sun, H.; Xu, Y.-P.; Nedaei, N. Multi-objective optimization and multi-aspect analysis of an innovative geothermal-based multi-generation energy system for power, cooling, hydrogen, and freshwater production. *Energy* **2022**, *245*, 123198. [[CrossRef](#)]
13. Musharavati, F.; Khanmohammadi, S.; Tariq, R. Comparative exergy, multi-objective optimization, and extended environmental assessment of geothermal combined power and refrigeration systems. *Process Saf. Environ. Prot.* **2021**, *156*, 438–456. [[CrossRef](#)]
14. Habibollahzade, A.; Mehrabadi, Z.K.; Markides, C.N. Comparative thermoeconomic analyses and multi-objective particle swarm optimization of geothermal combined cooling and power systems. *Energy Convers. Manag.* **2021**, *234*, 113921. [[CrossRef](#)]
15. Ansari, S.A.; Kazim, M.; Khaliq, M.A.; Ratlamwala, T.A.H. Thermal analysis of multigeneration system using geothermal energy as its main power source. *Int. J. Hydrogen Energy* **2021**, *46*, 4724–4738. [[CrossRef](#)]

16. Chaiyat, N. A multigeneration system of combined cooling, heating, and power (CCHP) for low-temperature geothermal system by using air cooling. *Therm. Sci. Eng. Prog.* **2021**, *21*, 100786. [[CrossRef](#)]
17. Cao, Y.; Ehyaei, M.A. Energy, exergy, exergoenvironmental, and economic assessments of the multigeneration system powered by geothermal energy. *J. Clean. Prod.* **2021**, *313*, 127823. [[CrossRef](#)]
18. Ansarinassab, H.; Hajabdollahi, H. Multi-objective optimization of a geothermal-based multigeneration system for heating, power and purified water production purpose using evolutionary algorithm. *Energy Convers. Manag.* **2020**, *223*, 113476. [[CrossRef](#)]
19. Ozturk, M.; Dincer, I. A new geothermally driven combined plant with energy storage option for six useful outputs in a sustainable community. *Sustain. Energy Technol. Assess.* **2021**, *45*, 101180. [[CrossRef](#)]
20. Islam, S.; Dincer, I. Development, analysis and performance assessment of a combined solar and geothermal energy-based integrated system for multigeneration. *Sol. Energy* **2017**, *147*, 328–343. [[CrossRef](#)]
21. Bamisile, O.; Huang, Q.; Dagbasi, M.; Adebayo, V.; Okonkwo, E.C.; Ayambire, P.; Al-Ansari, T.; Ratlamwala, T.A.H. Thermo-environment study of a concentrated photovoltaic thermal system integrated with Kalina cycle for multigeneration and hydrogen production. *Int. J. Hydrogen Energy* **2020**, *45*, 51, 26716–26732. [[CrossRef](#)]
22. Ratlamwala, T.A.H.; Waseem, S.; Salman, Y.; Bham, A.A. Geothermal and solar energy-based multigeneration system for a district. *Int. J. Energy Res.* **2019**, *43*, 5230–5251. [[CrossRef](#)]
23. Ebadollahi, M.; Rostamzadeh, H.; Pedram, M.Z.; Ghaebi, H.; Amidpour, M. Proposal and assessment of a new geothermal-based multigeneration system for cooling, heating, power, and hydrogen production, using LNG cold energy recovery. *Renew. Energy* **2019**, *135*, 66–87. [[CrossRef](#)]
24. Alirahmi, S.M.; Assareh, E.; Pourghassab, N.N.; Delpisheh, M.; Barelli, L.; Baldinelli, A. Green hydrogen & electricity production via geothermal-driven multi-generation system: Thermodynamic modeling and optimization. *Fuel* **2022**, *308*, 122049. [[CrossRef](#)]
25. Malik, M.; Dincer, I.; Rosen, M.A. Development and analysis of a new renewable energy-based multi-generation system. *Energy* **2015**, *79*, 90–99. [[CrossRef](#)]
26. Bozgeyik, A.; Altay, L.; Hepbasli, A. A sub-system design comparison of renewable energy based multi-generation systems: A key review along with illustrative energetic and exergetic analyses of a geothermal energy based system. *Sustain. Cities Soc.* **2022**, *82*, 103893. [[CrossRef](#)]
27. Suleman, F.; Dincer, I.; Agelin-Chaab, M. Development of an integrated renewable energy system for multigeneration. *Energy* **2014**, *78*, 196–204. [[CrossRef](#)]
28. Ghaebi, H.; Namin, A.S.; Rostamzadeh, H. Performance assessment and optimization of a novel multi-generation system from thermodynamic and thermo-economic viewpoints. *Energy Convers. Manag.* **2018**, *165*, 419–439. [[CrossRef](#)]
29. Yuksel, Y.E.; Ozturk, M.; Dincer, I. Development and assessment of a novel geothermal power-based multigenerational system with hydrogen and ammonia production options. *Energy Convers. Manag.* **2021**, *243*, 114365. [[CrossRef](#)]
30. Ratlamwala, T.A.H.; Dincer, I. Development of a geothermal based integrated system for building multigenerational needs. *Energy Build.* **2013**, *62*, 496–506. [[CrossRef](#)]
31. Mahmoud, M.; Ramadan, M.; Naher, S.; Pullen, K.; Abdelkareem, M.A.; Olabi, A.-G. A review of geothermal energy-driven hydrogen production systems. *Therm. Sci. Eng. Prog.* **2021**, *22*, 100854. [[CrossRef](#)]
32. Bicer, Y.; Dincer, I. Analysis and performance evaluation of a renewable energy based multigeneration system. *Energy* **2016**, *94*, 623–632. [[CrossRef](#)]
33. Heberle, F.; Brüggemann, D. Exergy based fluid selection for a geothermal Organic Rankine Cycle for combined heat and power generation. *Appl. Therm. Eng.* **2010**, *30*, 1326–1332. [[CrossRef](#)]
34. Bicer, Y.; Dincer, I. Development of a new solar and geothermal based combined system for hydrogen production. *Sol. Energy* **2016**, *127*, 269–284. [[CrossRef](#)]
35. Karapekmez, A.; Dincer, I. Thermodynamic analysis of a novel solar and geothermal based combined energy system for hydrogen production. *Int. J. Hydrogen Energy* **2020**, *45*, 5608–5628. [[CrossRef](#)]
36. Azhar, M.S.; Rizvi, G.; Dincer, I. Integration of renewable energy based multigeneration system with desalination. *Desalination* **2017**, *404*, 72–78. [[CrossRef](#)]
37. Yuksel, Y.E.; Ozturk, M.; Dincer, I. Energetic and exergetic assessments of a novel solar power tower based multigeneration system with hydrogen production and liquefaction. *Int. J. Hydrogen Energy* **2019**, *44*, 13071–13084. [[CrossRef](#)]
38. Ganjehsarabi, H. Mixed refrigerant as working fluid in Organic Rankine Cycle for hydrogen production driven by geothermal energy. *Int. J. Hydrogen Energy* **2019**, *44*, 18703–18711. [[CrossRef](#)]
39. Siddiqui, O.; Ishaq, H.; Dincer, I. A novel solar and geothermal-based trigeneration system for electricity generation, hydrogen production and cooling. *Energy Convers. Manag.* **2019**, *198*, 111812. [[CrossRef](#)]
40. Liu, Q.; Shang, L.; Duan, Y. Performance analyses of a hybrid geothermal–fossil power generation system using low-enthalpy geothermal resources. *Appl. Energy* **2016**, *162*, 149–162. [[CrossRef](#)]
41. Gholizadeh, T.; Vajdi, M.; Rostamzadeh, H. A new trigeneration system for power, cooling, and freshwater production driven by a flash-binary geothermal heat source. *Renew. Energy* **2020**, *148*, 31–43. [[CrossRef](#)]
42. Rostamzadeh, H.; Gargari, S.G.; Namin, A.S.; Ghaebi, H. A novel multigeneration system driven by a hybrid biogas-geothermal heat source, Part I: Thermodynamic modeling. *Energy Convers. Manag.* **2018**, *177*, 535–562. [[CrossRef](#)]

43. Waseem, S.; Ratlamwala, T.A.H.; Salman, Y.; Bham, A.A. Geothermal and solar based mutligenerational system: A comparative analysis. *Int. J. Hydrogen Energy* **2020**, *45*, 5636–5652. [[CrossRef](#)]
44. Geothermal Energy Knowledge. Available online: <https://eniscuola.eni.com/en-IT/energy/geothermal/geothermal-energy-knowledge.html> (accessed on 8 January 2023).

**Disclaimer/Publisher’s Note:** The statements, opinions and data contained in all publications are solely those of the individual author(s) and contributor(s) and not of MDPI and/or the editor(s). MDPI and/or the editor(s) disclaim responsibility for any injury to people or property resulting from any ideas, methods, instructions or products referred to in the content.